International Journal of Mechanical Engineering (IJME)
ISSN(P): 2319-2240; ISSN(E): 2319-2259
Vol. 4, Issue 5, Aug- Sep 2015, 25-36

International Academy of Science, Engineering and Technology
Connecting Researchers; Nurturing Innovations

EFFECTS OF ADHESIVE AND INTERPHASE CHARACTERISTICS BETWEEN MATRIX AND REINFORCED NANOPARTICLE OF AA3105/ALN NANOCOMPOSITES

A. CHENNAKESAVA REDDY

Professor, Department of Mechanical Engineering, JNTUH College of Engineering, Hyderabad, India

ABSTRACT

Adhesion between nanoparticles and metal matrix can affect a composite's mechanical properties. Decreasing the interfacial strength can cause the interfacial debonding of particles from the matrix and, as a consequence, the tensile strength of the composite is reduced. In this article two types of RVE models have been implemented to study adhesive characteristics between aluminum nitride (AlN) nanoparticle and AA3105 matrix using finite element analysis. It has been observed that the nanoparticle did not overload during the transfer of load from the matrix to the nanoparticle via the interphase due to interphase between the nanoparticle and the matrix. The tensile strength and elastic modulus has been found increasing with an increase volume fraction of aluminum nitride in the AA3105/AlN nanocomposites. The transverse modulus of AlN/AA3105 nanocomposites is increased from 74.84 to 83.25 GPa with interphase due to addition of magnesium.

KEYWORDS: RVE Models, Aln, AA3105, Finite Element Analysis, Interphase

INTRODUCTION

During the past several decades composite materials are finding increasing use in a variety of application such as aircraft, automobiles, etc. The higher stiffness of ceramic particles can lead to an incremental increase in the stiffness of a composite [1, 2]. One of the major challenges when processing nanocomposites is achieving a homogeneous distribution of reinforcement in the matrix as it has a strong impact on the properties and the quality of the material. The current processing methods often generate agglomerated particles in the ductile matrix and as a result they exhibit extremely low ductility [3]. Particle clusters act as crack or decohesion nucleation sites at stresses lower than the matrix yield strength, causing the nanocomposite to fail at unpredictable low stress levels. Possible reasons resulting in particle clustering are chemical binding, surface energy reduction or particle segregation [4, 5, 6]. While manufacturing Al alloy-AlN nanocomposites, the wettability factor is the main concern irrespective of the manufacturing method. Its high surface activity restricts its incorporation in the metal matrix. One of the methods is to add surfactant which acts as a wetting agent in molten metal to enhance wettability of particulates. Researchers have successfully used several surfactants like Li, Mg, Ca, Zr, Ti, Cu, and Si for the synthesis of nanocomposites [7, 8, 9].

The objective of this article was to develop AA3015/AlN nanocomposites with and without wetting criteria of AlN by AA3015 molten metal. The RVE models were used to analyze the nanocomposites using finite Element analysis. A homogeneous interphase region was assumed in the models. The results obtained from the finite element analysis were verified with those obtained from the experimentation.

THEORETICAL BACKGROUND

Analyzing structures on a microstructural level, however, is clearly an inflexible problem. Analysis methods have therefore sought to approximate composite structural mechanics by analyzing a representative section of the composite microstructure, commonly called a Representative Volume Element (RVE). One of the first formal definitions of the RVE was given by Hill [10] who stated that the RVE was 1) structurally entirely typical of the composite material on average and 2) contained a sufficient number of inclusions such that the apparent moduli were independent of the RVE boundary displacements or tractions. Under axisymmetric as well as antisymmetric loading, a 2-D axisymmetric model can be applied for the cylindrical RVE, which can significantly reduce the computational work [11].

Determination Effective Material Properties

To derive the formulae for deriving the equivalent material constants, a homogenized elasticity model of the square representative volume element (RVE) as shown in figure 1 is considered. The dimensions of the three-dimensional RVE are 2*a* x 2*a* x 2*a*. The cross-sectional area of the RVE is 2*a* x 2*a*. The elasticity model is filled with a single, transversely isotropic material that has five independent material constants (elastic moduli E_y and E_z, Poison's ratios v_{xy}, v_{yz} and shear modulus G_{yz}). The general strain-stress relations relating the normal stresses and the normal stains are given below:

$$\varepsilon_x = \frac{\sigma_x}{E_x} - \frac{v_{xy}\sigma_y}{E_y} - \frac{v_{xz}\sigma_z}{E_z} \tag{1}$$

$$\varepsilon_y = -\frac{v_{yx}\sigma_x}{E_y} + \frac{\sigma_y}{E_y} - \frac{v_{yz}\sigma_z}{E_z} \tag{2}$$

$$\varepsilon_z = -\frac{v_{zx}\sigma_x}{E_x} - \frac{v_{zy}\sigma_y}{E_y} + \frac{\sigma_z}{E_z} \tag{3}$$

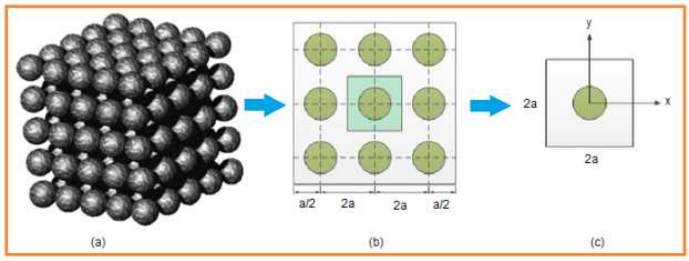

Figure 1: A square RVE Containing a Nanoparticle

Let assume that $\sigma_{xy} = \sigma_{yx}, \sigma_{yz} = \sigma_{zy}$ and $\sigma_{zx} = \sigma_{xz}$. For plane strain conditions, $\epsilon_z = 0, \epsilon_{yz} = \varepsilon_{zx} = 0$ and $v_{yz} = v_{zx}$. The above equations are rewritten as follows:

$$\varepsilon_x = \frac{\sigma_x}{E_x} - \frac{v_{xy}\sigma_y}{E_y} - \frac{v_{yz}\sigma_z}{E_z} \tag{4}$$

$$\varepsilon_y = -\frac{v_{xy}\sigma_x}{E_y} + \frac{\sigma_y}{E_y} - \frac{v_{yz}\sigma_z}{E_z} \tag{5}$$

$$\varepsilon_z = -\frac{v_{yz}\sigma_x}{E_z} - \frac{v_{yz}\sigma_y}{E_z} + \frac{\sigma_z}{E_z} \tag{6}$$

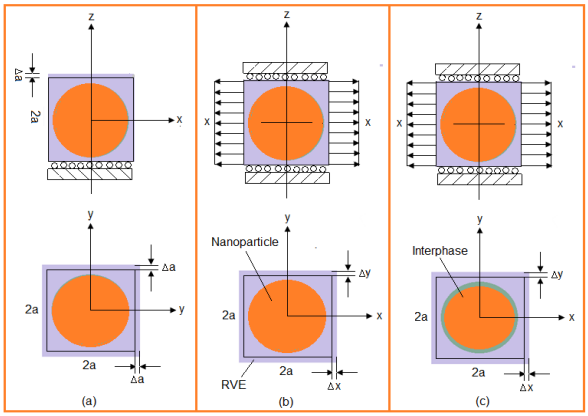

Figure 2: RVE Models

To determine E_y and E_z, v_{xy} and v_{yz}, four equations are required. Two loading cases as shown in figure 2 have been designed to give four such equations based on the theory of elasticity. For load case (figure 2a), the stress and strain components on the lateral surface are:

$$\sigma_x = \sigma_y = 0$$

$$\varepsilon_x = \frac{\Delta a}{a} \text{ along } x = \pm a \text{ and } \varepsilon_y = \frac{\Delta a}{a} \text{ along } y = \pm a$$

$$\varepsilon_z = \frac{\Delta a}{a}$$

Where Δa is the change of dimension a of cross-section under the stretch Δa in the z-direction. Integrating and averaging Eq. (6) on the plane $z = a$, the following equation can be arrived:

$$E_z = \frac{\sigma_{ave}}{\varepsilon_z} = \frac{a}{\Delta a}\sigma_{ave} \tag{7}$$

Where the average value of σ_z is given by:

$$\sigma_{ave} = \iint \sigma_z(x, y, a)dxdy \tag{8}$$

The value of σ_{ave} is evaluated for the RVE using finite element analysis (FEA) results.

Using Eq. (5) and the result (7), the strain along $y = \pm a$:

$$\varepsilon_y = -\frac{v_{yz}\sigma_z}{E_z} = -v_{yz}\frac{\Delta a}{a} = \frac{\Delta a}{a}$$

Hence, the expression for the Poisson's ratio vyz is as follows:

$$v_{yz} = -1 \tag{9}$$

For load case (figure 2b), the square representative volume element (RVE) is loaded with a uniformly distributed load (negative pressure), P in a lateral direction, for instance, the x-direction. The RVE is constrained in the z-direction so that the plane strain condition is sustained to simulate the interactions of RVE with surrounding materials in the z-direction. Since $\varepsilon_z = 0$, $\sigma_z = v_{yz}(\sigma_x + \sigma_y)$ for the plain stress, the strain-stress relations can be reduced as follows:

$$\varepsilon_x = \left(\frac{1}{E_x} - \frac{1}{E_z}\right)\sigma_x - \left(\frac{v_{xy}}{E_y} + \frac{1}{E_z}\right)\sigma_y \tag{10}$$

$$\varepsilon_y = -\left(\frac{v_{xy}}{E_x} + \frac{1}{E_z}\right)\sigma_x + \left(\frac{1}{E_x} - \frac{1}{E_z}\right)\sigma_y \quad (11)$$

For the elasticity model as shown in figure 2b, one can have the following results for the normal stress and strain components at a point on the lateral surface:

$\sigma_y = 0, \sigma_x = P$

$\varepsilon_x = \frac{\Delta x}{a}$ along $x = \pm a$ and $\varepsilon_y = \frac{\Delta y}{a}$ along $y = \pm a$

Where Δx (>0) and Δy (<0) are the changes of dimensions in the x- and y- direction, respectively for the load case shown in figure 2b. Applying Eq. (11) for points along $y = \pm a$ and Eq. (10) for points along $x = \pm a$, we get the following:

$$\varepsilon_y = -\left(\frac{v_{xy}}{E_x} + \frac{1}{E_z}\right)P = \frac{\Delta y}{a} \quad (12)$$

$$\varepsilon_x = \left(\frac{1}{E_x} - \frac{1}{E_z}\right)P = \frac{\Delta x}{a} \quad (13)$$

By solving Eqs. (12) and (13), the effective elastic modulus and Poisson's ratio in the transverse direction (xy-plane) as follows:

$$E_x = E_y = \frac{1}{\frac{\Delta x}{Pa} + \frac{1}{E_z}} \quad (14)$$

$$v_{xy} = -\left(\frac{\Delta y}{Pa} + \frac{1}{E_z}\right)/\left(\frac{\Delta x}{Pa} + \frac{1}{E_z}\right) \quad (15)$$

In which E_z can be determined from Eq. (7). Once the change in lengths along x- and y- direction (Δx and Δy) are determined for the square RVE from the FEA, E_y (= E_x) and v_{xy} can be determined from Eqs. (14) and (15), correspondingly.

Empirical Models for Elastic Moduli and Strength of Nanocomposites

The strength of a particulate metal matrix composite depends on the strength of the weakest zone and metallurgical phenomena in it [12, 13]. A new criterion is suggested by the author considering adhesion, formation of precipitates, particle size, agglomeration, voids/porosity, obstacles to the dislocation, and the interfacial reaction of the particle/matrix. The formula for the strength of composite is stated below:

$$\sigma_c = \left[\sigma_m \left\{\frac{1-(v_p+v_v)^{2/3}}{1-1.5(v_{p+}v_v)}\right\}\right] e^{m_{p(v_p+v_v)}} + k d_p^{-1/2} \quad (16)$$

$, k = E_m m_m / E_p m_p$

where, v_v and v_p are the volume fractions of voids/porosity and nanoparticles in the composite respectively, m_p and m_m are the possion's ratios of the nanoparticles and matrix respectively, d_p is the mean nanoparticle size (diameter) and E_m and E_p is elastic moduli of the matrix and the particle respectively. Elastic modulus (Young's modulus) is a measure of the stiffness of a material and is a quantity used to characterize materials. Elastic modulus is the same in all orientations for isotropic materials. Anisotropy can be seen in many composites. The proposed equations [12, 13] by the author to find Young's modulus of composites and interphase including the effect of voids/porosity as given below:

The upper-bound equation is given by

$$\frac{E_c}{E_m} = \left(\frac{1-{v_v}^{2/3}}{1-{v_v}^{2/3}+v_v}\right) + \frac{1+(\delta-1){v_p}^{2/3}}{1+(\delta-1)({v_p}^{2/3}-v_p)} \quad (17)$$

The lower-bound equation is given by

$$\frac{E_c}{E_m} = 1 + \frac{v_{p-}v_p}{\delta/(\delta-1)-(v_p+v_{v)}{}^{1/3}} \quad (18)$$

Where, $\delta = E_p/E_m$.

The transverse modulus is given by

$$\mathrm{E_t} = \frac{E_m E_p}{E_m + E_p(1-{v_p}^{2/3})/{v_p}^{2/3}} + E_m\left(1-{v_p}^{2/3}-{v_v}^{2/3}\right) \quad (19)$$

The young's modulus of the interphase is obtained by the following formula:

$$E_i(r) = \left(\alpha E_p - E_m\right)\left(\frac{r_i-r}{r_i-r_p}\right) + E_m \quad (20)$$

MATERIALS METHODS

The matrix material was AA3105 aluminum alloy. AA3105 contains Si (0.60%), Cu (0.30%), Cr (0.20%), Fe (0.70%), Mn (0.15%) and Mg (0.50%) as its major alloying elements. The reinforcement material was aluminum nitride (AlN) nanoparticles of average size 100nm. The mechanical properties of materials used in the present work are given in table 1.

Table 1: Mechanical Properties of AA3105 Matrix and AlN Nanoparticles

Property	AA3105	AlN
Density, g/cc	2.72	3.26
Elastic modulus, GPa	68.9	330
Ultimate tensile strength, MPa	214	270
Poisson's ratio	0.33	0.24

Preparation of Composite Specimens

The matrix alloys and composites were prepared by the stir casting and low-pressure die casting process. The volume fractions of carbon black reinforcement were 10%, 20%, and 30%. AA3105 matrix alloy was melted in a resistance furnace. The crucibles were made of graphite. The melting losses of the alloy constituents were taken into account while preparing the charge. The charge was fluxed with coverall to prevent dressing. The molten alloy was degasified by tetrachlorethane (in solid form). The crucible was taken away from the furnace; and the melt was treated with sodium modifier. Then the liquid melt was allowed to cool down just below the liquidus temperature to get the melt semi solid state. At this stage, the preheated (500^0C for 1 hour) reinforcement particles and magnesium as a wetting agent were added to the liquid melt. The molten alloy and reinforcement particles are thoroughly stirred manually for 15 minutes. After manual steering, the semi-solid, liquid melt was reheated, to a full liquid state in the resistance furnace followed by an automatic mechanical stirring using a mixer to make the melt homogenous for about 10 minutes at 200 rpm. The temperature of melted metal was measured using a dip type thermocouple. The preheated cast iron die was filled with dross-removed melt by the compressed (3.0 bar) argon gas [1, 2].

Heat Treatment

Prior to the cold rolling of composite samples, a solution treatment was applied at 345^0C for 1 hour, followed by quenching in cold water. The samples were cold rolled to 2% reduction in a laboratory mill a relatively low strain rate, probably less than 1. Lubricated rolls were used at maximum speed. The strain was calculated from the thicknesses of the test samples before and after rolling process.

Tensile Tests

The heat-treated samples were machined to get flat-rectangular specimens (figure 3) for the tensile tests. The tensile specimens were placed in the grips of a Universal Test Machine (UTM) at a specified grip separation and pulled until failure. The test speed was 2 mm/min (as for ASTM D3039). A strain gauge was used to determine elongation.

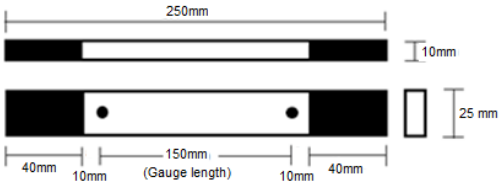

Figure 3: Shape and Dimensions of Tensile Specimen

Optical and Scanning Electron Microscopic Analysis

An image analyzer was used to study the distribution of the AlN reinforcement particles within the AA3015 matrix. The polished specimens were ringed with distilled water, and etched with a solution (distilled water: 190 ml, nitric acid: 5ml, hydrochloric acid: 3 ml and hydrofluoric acid: 2 ml) for optical microscopic analysis. Fracture surfaces of the deformed/fractured test samples were analyzed with a scanning electron microscope (SEM) to define the macroscopic fracture mode and to establish the microscopic mechanisms governing fracture. Samples for SEM observation were obtained from the tested specimens by sectioning parallel to the fracture surface and the scanning was carried using S-3000N Toshiba SEM.

Finite Element Analysis (FEA)

The representative volume element (RVE or the unit cell) is the smallest volume over which a measurement can be made that will yield a value representative of the whole. In this research, a cubical RVE was implemented to analyze the tensile behavior AA3015/AlN nanocomposites (figure 6). The determination of the RVE's dimensional conditions requires the establishment of a volumetric fraction of spherical nanoparticles in the composite. Hence, the weight fractions of the particles were converted to volume fractions. The volume fraction of a particle in the RVE ($v_{p,\text{rve}}$) is determined using Eq.(21):

$$v_{p,rve} = \frac{\text{Volume of nanoparticle}}{\text{Volume of RVE}} = \frac{16}{3} \times \left(\frac{r}{a}\right)^3 \tag{21}$$

Where, r represents the particle radius and a indicates the diameter of the cylindrical RVE. The volume fraction of the particles in the composite (V_p) is obtained using equation

$$V_p = (w_p/\rho_p)/(w_p/\rho_p + w_m/\rho_m) \tag{22}$$

Where ρ_m and ρ_p denote the matrix and particle densities, and w_m and w_p indicate the matrix and particle weight fractions, respectively.

The RVE dimension (a) was determined by equalizing Eqs. (21) and (22). Two RVE schemes namely: without interphase (adhesion) and with interphase were applied between the matrix and the filler. The loading on the RVE was defined as symmetric displacement, which provided equal displacements at both ends of the RVE. To obtain the nanocomposite modulus and yield strength, the force reaction was defined against displacement. The large strain PLANE183 element [14] was used in the matrix and the interphase regions in all the models. In order to model the adhesion between the interphase and the particle, a COMBIN14 spring-damper element was used. The stiffness of this element was taken as unity for perfect adhesion which could determine the interfacial strength for the interface region.

To converge an exact nonlinear solution, it is also important to set the strain rates of the FEM models based on the experimental tensile tests' setups. Hence, FEM models of different RVEs with various particle contents should have comparable error values. In this respect, the ratio of the tensile test speed to the gauge length of the specimens should be equal to the corresponding ratio in the RVE displacement model. Therefore, the rate of displacement in the RVEs was set to be 0.1 (1/min).

RESULTS AND DISCUSSIONS

Figure 4 reveals the microstructure of AA3015/AlN nanocomposite wherein the AlN nanoparticles are distributed in the AA3015 matrix uniformly (approximated).

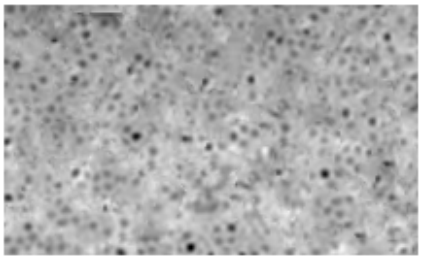

Figure 4: AlN (30%Vp) Nanoparticle Distribution in AA3015 Matrix

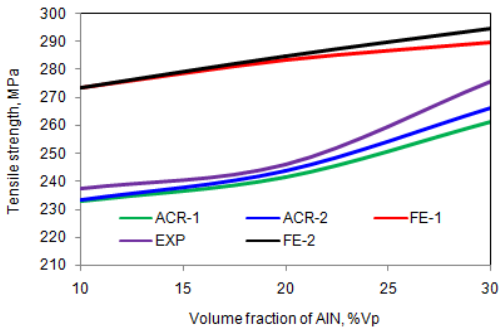

Figure 5: Effect of Volume Fraction on Tensile Strength along Tensile Load Direction

Tensile Behavior

An increase of AlN content in the matrix could increase the tensile strength of the nanocomposite (figure 5). The maximum difference (36.03 MPa) between the FEA results without interphase and the experiments results can be attributed to lack of bonding between the AlN nanoparticle and the AA3015 matrix. The discrepancy (35.88 MPa) between the FEA results with interphase and the experiments results can be endorsed to the micro-metallurgical factors (such as formation of voids and nanoparticle clustering) that were not considered in the RVE models. Author's model includes the

effect of voids present in the nanocomposite. The results obtained from author's model (with voids) were nearly equal to the experimental values with maximum deviation of 4.25 MPa.

For 10%, 20% and 30%Vp of AlN in AA3015, without interphase and barely consideration of adhesive bonding between the AlN nanoparticle and the AA3015 matrix, the loads transferred from the AlN nanoparticle to the AA3015 matrix were, respectively, 44.20 MPa, 68.47 MPa and 69.49 MPa (figure 6a) along the tensile load direction. Likewise, for 10%, 20% and 30%Vp of AlN in AA2124, with interphase and wetting between the ALN nanoparticle and the AA3015 matrix, the loads transferred from the AlN nanoparticle to the AA3015 matrix were, respectively, 67.05 MPa, 88.32 MPa and 91.06 MPa (figure 6c) along the tensile load direction. Zhengang et al [15] carried a study improving wettability by adding Mg as the wetting agent. They suggested that the wettability between molten Al-Mg matrix and SiC particles is improved and the surface tension of molten Al-Mg alloy with SiC particle is reduced, and results in homogeneous particles distribution and high interfacial bond strength. For instance, addition of Mg to composite matrix lead to the formation of MgO and $MgAl_2O_3$ at the interface and this enhances the wettability and the strength of the composite [16]. The stresses induced in the normal direction to loading were lower than those induced along the load direction (figure 6b and 6d). The combination of tensile and compressive stresses was induced in the normal direction of loading.

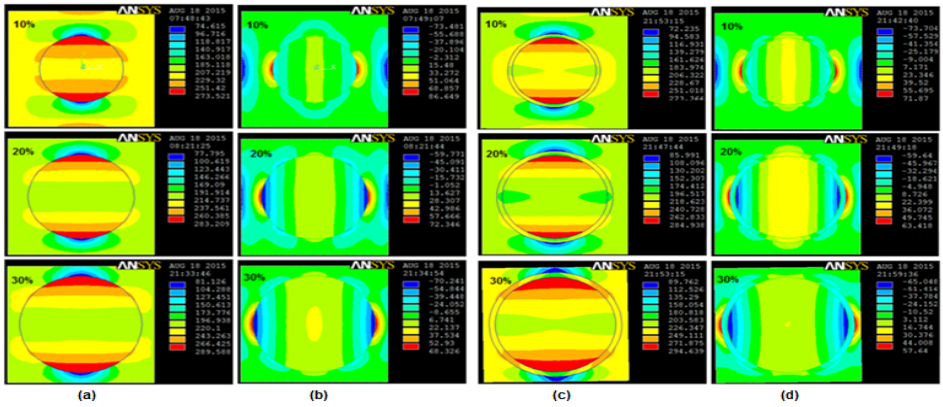

Figure 6: Tensile Stresses (a) without Interphase, Parallel, (b) with Interphase, Normal, (c) without Interphase, Parallel and (d) with Interphase, Normal to Load Direction

The strains along the load direction were higher than those in the normal direction (figure 7). Accordingly, the RVE was expanded elastically away from the particle in the direction of the tensile loading. This would increase the contact area between the particle and the matrix in the perpendicular direction to the tensile loading and would decrease the contact area between the particle and the matrix in the direction of the tensile loading. For the nanocomposites with and without interphase the only difference was the propagation of deformation from the matrix to the nanoparticle. This washigh with interphase as it would improve the wettability of the nanoparticle with the matrix. The interphase extends theyielding character of the nano composite.

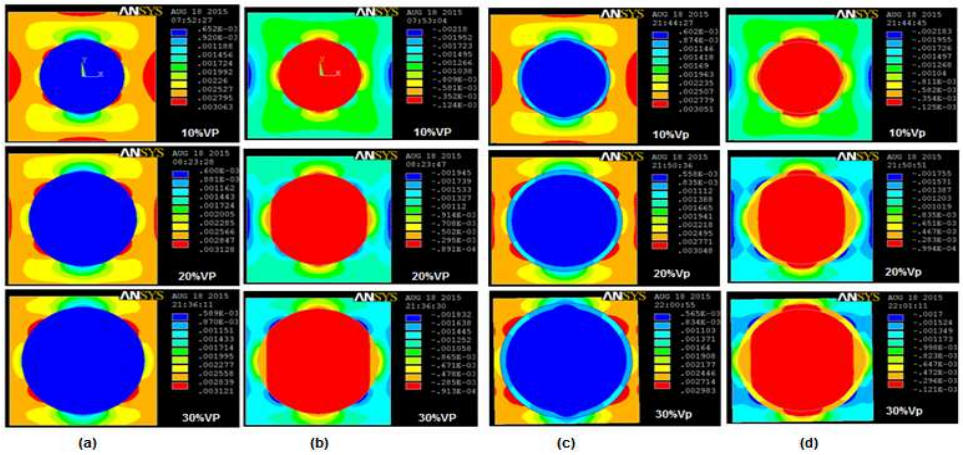

Figure 7: Elastic Strain (a) without Interphase, Parallel, (b) with Interphase, Normal, (c) without Interphase, Parallel and (d) with Interphase, Normal to Load Direction

Table 2: Elastic Moduli of AA3105/AlN Nano Composite

Source	Criteria	Longitudinal Elastic Modulus, GPa			Transverse Elastic Modulus, GPa		
		Vp = 10%	Vp = 20%	Vp = 30%	Vp = 10%	Vp = 20%	Vp = 30%
FEA	without interphase	89.26	92.54	90.75	89.35	92.64	90.85
FEA	with interphase	93.26	96.62	91.61	93.36	96.72	91.72
Author	upper limit	163.54	179.28	195.19	72.39	77.62	84.94
Author	lower limit	78.21	84.12	90.16	-	-	-
Rule of Mixture		98.79	124.48	150.17	79.27	86.58	95.37

Table 3: Poisson's Ratios

	Without Interphase			With Interphase		
Poisson's Ratio	Vp = 10%	Vp = 20%	Vp = 30%	Vp = 10%	Vp = 20%	Vp = 30%
v_{xy}	0.9997	0.9996	0.9996	0.9996	0.9996	0.9995
v_{yz}	-1	-1	-1	-1	-1	-1
v_{zx}	-1	-1	-1	-1	-1	-1

The tensile elastic modulus increased appreciably with interphase around the AlN nanoparticle (table 2). The results of longitudinal moduli obtained FEA were within the limits of author's models. Due to existence of voids in the nanocomposites, the elastic moduli were closer lower limit. The transverse moduli obtained by FEA were higher than the results obtained by the author's models and the Rule of Mixture. The elastic moduli along longitudinal and transverse directions were nearly equal, respectively, with the interphase and without interphase around the AlN nanoparticle. The Poisson's ratios $v_{xy,}$ v_{yz} and v_{zx} were also nearly equal (table 3). Hence, it is proved the assumptions of isotropic conditions while deriving the mathematical models in this paper. The FEA procedure adopted and the empirical models are also proven acceptable as the results are within tolerable limits.

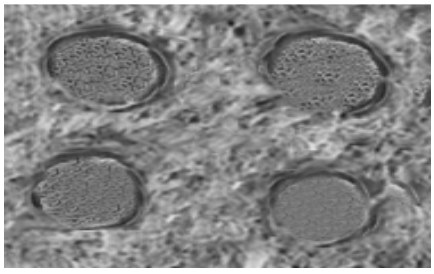

Figure 8: Interphase between AlN Nanoparticle and AA3105 Matrix

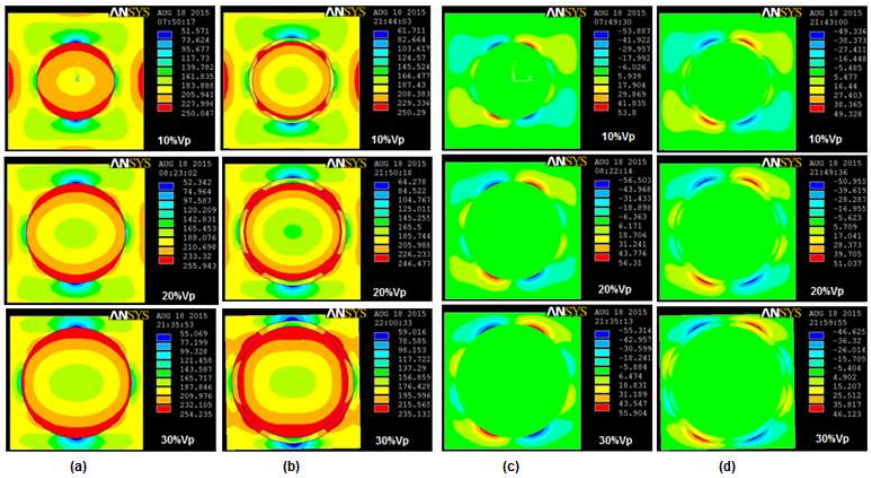

Figure 9: von Mises Stress (a) without Interphase, (b) with Interphase and Shear Stress (c) without Interphase (d) with Interphase

Fracture

There is a clear existence of interphase between the AlN nanoparticle and AA3105 matrix as shown in figure 8. Mg leads to the formation of MgO and $MgAl_2O_3$ at the matrix-reinforcement interface [16]. The phases Al_2Cu, Al_5Mg_8 are also observed in the microstructures. Hashin put the interface model into physical terms for composites [17]. The effect of the interphase is modeled by allowing displacement discontinuities at the 2D interface that are linearly related to the stress in each displacement direction. The von Mises stresses for the nanocomposites having interphase were lower than those for the nanocomposites without interphase (figure 9). The adhesion strength at the interface determines the load transfer between the components. For poorly bonded particles, the stress transfer at the particle/matrix interface is inefficient. Discontinuities in the form of debonding were observed in the nanocomposites without interphase because of non-adherence of the nano particle to the matrix. The shear stresses induced in the nanocomposites with and without interphase are shown in figure 10. In the case of nanocomposites with interphase between the nanoparticle and the matrix, the stress is transferred through shear from the matrix to the particles. Hence, the stress transfer from the matrix to the nanoparticle becomes less for the nanocomposites without interphase resulting high stress in the matrix. Landis and McMeeking [18] assume that the fibers carry the entire axial load, and the matrix material only transmits shear between the fibers. Based on these assumptions alone, it is generally accepted that these methods will be most accurate when the fiber volume fraction V_f and the fiber-to matrix moduli ratio E_f/E_m are high. In the present case the elastic moduli of AlN nano particle and AA3105 matrix are, respectively, 330 GPa and 68.9 GPa.

CONCLUSIONS

Without interphase around AlN nanoparticles, the tensile strength has been found to be 289.59 MPa for the nanocomposites consisting of 30% volume fraction. Due to interphase between the nanoparticle and the matrix, the tensile strength increases to 294.64 MPa. The tensile strengths obtained by author's model (with voids) are in good agreement with the experimental results. In the case of nanocomposites with interphase between the nanoparticle and the matrix, the stress is transferred through shear from the matrix to the particles through interphase. The transverse moduli of AlN/AA3105 nanocomposites have been found to be 74.84 GPa and 83.25 GPa, respectively, without and with interphase.

ACKNOWLEDGEMENTS

The author thanks the University Grants Commission (UGC), New Delhi for sanctioning this major project. The author also thanks the Central University, Hyderabad for providing the SEM images to complete this manuscript.

REFERENCES

1. A. Chennakesava Reddy, "Mechanical properties and fracture behavior of 6061/SiCp Metal Matrix Composites Fabricated by Low Pressure Die Casting Process," Journal of Manufacturing Technology Research, vol.1(3/4), pp. 273-286, 2009.
2. A. Chennakesava Reddy and Essa Zitoun, "Tensile properties and fracture behavior of 6061/Al_2O_3 metal matrix composites fabricated by low pressure die casting process," International Journal of Materials Sciences, vol. 6(2), pp. 147-157, 2011.
3. X. Deng and N. Chawla, "Modeling the effect of particle clustering on the mechanical behavior of SiC particle reinforced Al matrix composites," Journal of Materials Science, vol.41, pp.5731–5734, 2006.
4. A.J. Reeves, H. Dunlop and T.W. Clyne, "The effect of interfacial reaction layer thickness on fracture of titanium–SiC particulate composites," Metallurgical Transactions A, vol.23, pp.977–988, 1992.
5. B. Kotiveerachari, A, Chennakesava Reddy, "Interfacial effect on the fracture mechanism in GFRP composites," CEMILAC Conference, Ministry of Defense, India 1(b), pp.85-87, 1999.
6. A. Chennakesava Reddy, "Analysis of the Relationship Between the Interface Structure and the Strength of Carbon-Aluminum Composites," NATCON-ME, Bangalore, 13-14th March, pp.61-62, 2004.
7. S. Ren, X. Shen, X. Qu and X. He, "Effect of Mg and Si on infiltration behavior of Al alloys pressureless infiltration into porous SiCp preforms," International Journal Minerals, Metallurgy and Materials, vol.18 (6), pp.703–708, 2011.
8. N. Sobczak, M. Ksiazek, W. Radziwill, J. Morgiel, W. Baliga and L. Stobierski, "Effect of titanium on wettability and interfaces in the Al/ SiC system," in: Proceedings of the International Conference High Temperature Capillarity, Cracow, Poland, 29 June–2 July 1997.
9. A.M. Davidson and D. Regener, "A comparison of aluminum based metal matrix composites reinforced with coated and uncoated particulate silicon carbide," Composites Science and Technology, vol.60(6), pp.865-869, 2000.
10. R. Hill, "Elastic properties of reinforced solids: some theoretical principles," Journal of the Mechanics and Physics of Solids, vol.11, pp.357-372, 1963.
11. Y.J. Liu and X.L. Chen, "Evaluations of the effective material properties of carbon nanotube-based composites using a nanoscale representative volume element", Mechanics of Materials, vol.35, pp.69–81, 2003.
12. A. Chennakesava Reddy, "Cause and Catastrophe of Strengthening Mechanisms in 6061/Al2O3 Composites Prepared by Stir Casting Process and Validation Using FEA," International Journal of Science and Research, vol.4(2), pp.1272-1281, 2015.

13. A. Chennakesava Reddy, “Influence of Particle Size, Precipitates, Particle Cracking, Porosity and Clustering of Particles on Tensile Strength of 6061/SiCp Metal Matrix Composites and Validation Using FEA,” International Journal of Material Sciences and Manufacturing Engineering,” vol.42(1), pp.1176-1186, 2015.
14. Chennakesava R Alavala, “Finite element methods: Basic concepts and applications,” PHI Learning Pvt. Ltd, New Delhi, 2008.
15. Zhengang Liuy, Guoyin Zu, Hongjie Luo, Yihan Liu and Guangchun Yao, “Influence of Mg Addition on Graphite Particle Distribution in the Al Matrix Composites,” Journal of Materials Science & Technology, vol.26 (3), pp.244-pp.244-250, 2010.
16. A. Chennakesava Reddy and Essa Zitoun, “Matrix alloys for alumina particle reinforced metal matrix composites,” Indian Foundry Journal,vol.55(1), pp.12-16, 2009.
17. Z. Hashin, “Thermoelastic Properties of Fiber Composites With Imperfect Interface," Mechanics of Materials, vol.8, pp. 333-348, 1990.
18. C.M. Landis and R.M. McMeeking, “Stress concentrations in composites with interface sliding, matrix stiffness, and uneven fiber spacing using shear lag theory,” n International Journal of Solids Structures, vol.41, pp. 6289-6313, 1999.